Available online at www.sciencedirect.com
SCIENCE DIRECT
Journal of Power Sources 154 (2006) 124–137
JOURNAL OF POWER SOURCES
www.elsevier.com/locate/jpowsour

Liquid water transport in parallel serpentine channels with manifolds on cathode side of a PEM fuel cell stack

Kui Jiao, Biao Zhou*, Peng Quan

Department of Mechanical, Automotive and Materials Engineering, University of Windsor, Ont., Canada N9B 3P4

Received 2 March 2005; accepted 1 April 2005
Available online 31 May 2005

Abstract

Water management in a proton exchange membrane (PEM) fuel cell stack has been a challenging issue on the road to commercialization. This paper presents a numerical investigation of air–water flow in parallel serpentine channels on cathode side of a PEM fuel cell stack by use of the commercial Computational Fluid Dynamics (CFD) software package FLUENT. Different air–water flow behaviours inside the serpentine flow channels with inlet and outlet manifolds were discussed. The results showed that there were significant variations of water distribution and pressure drop in different cells at different times. The "collecting-and-separating effect" due to the serpentine shape of the gas flow channels, the pressure drop change due to the water distribution inside the inlet and outlet manifolds were observed. Several gas flow problems of this type of parallel serpentine channels were identified and useful suggestions were given through investigating the flow patterns inside the channels and manifolds.

Keywords: Water management; Proton exchange membrane; Pressure drop; Parallel serpentine channels; Air–water behaviour; CFD modeling

1. Introduction

Low operating temperature and zero/low emission have made Polymer Electrolyte Membrane (PEM) fuel cells become the most promising power source for the future in vehicle and portable applications [1]. However, to achieve commercialization, the performance of PEM fuel cells needs to be improved by proper engineering design and optimization. Due to the special chemical structure of the PEM, the membrane must be well hydrated to ensure that a sufficient amount of hydrogen ions could cross. On the other hand, due to the low operating temperature of PEM fuel cells (30–100 °C) [1], excessive humidification could result in water vapour condensation that could subsequently block the gas flow channels resulting in a lower air flow rate on the cathode side, thus decreasing fuel cell performance. Water content is also an important factor that affects the ohmic resistance in the membrane [2]. Therefore, keeping an appropriate amount of water content in the fuel cell to avoid both membrane dehydration and water vapour condensation has been a critical issue in improving fuel cell performance. In reality, however, it is almost impossible to manage water on both the anode and cathode sides without dehydration and condensation, this is simply because water vapour condensation in the gas flow channels of practical fuel cell applications is unavoidable [2]. Therefore, water management, to which many engineers and scientists have recently paid particular attention, has been a critical challenge for a high-performance fuel cell design and optimization.

In the last decade, water management related studies were performed numerically and experimentally for different purposes and in several ways. A three-dimensional (3D) numerical simulation of a straight gas flow channel in a PEM fuel cell was performed by Dutta et al. [3] using a commercial CFD software FLUENT. They found that membrane thickness, cell voltage and current density could affect water trans-

* Corresponding author. Tel.: +1 519 253 3000x2630; fax: +1 519 973 7007.
E-mail address: bzhou@uwindsor.ca (B. Zhou).

0378-7753/$ – see front matter © 2005 Elsevier B.V. All rights reserved.
doi:10.1016/j.jpowsour.2005.04.003

port across the membrane. Hontanon et al. [4] also employed FLUENT to implement their 3D, stationary gas flow model. A study exploring the steady-state gas transport phenomena in micro-scale parallel flow channels was conducted by Cha et al. [5] in which oxygen concentration along a single gas flow channel and other flow patterns that may affect fuel cell performance were discussed. Similarly, gas concentration of a steady-state flow along fuel cell flow channels was obtained numerically by Kulikovsky [6]. Djilali and co-workers [7] proposed a 3D CFD model of a PEM fuel cell with serpentine flow channels. Their model accounts for the major transport phenomena in a PEM fuel cell. However, in all the studies mentioned above, the effects of liquid water were neglected. Yi et al. [2] pointed out that water vapour condensation was inevitable on both the anode and cathode sides of a PEM fuel cell, and they discussed a liquid water removal technique that used a water transport plate to lead excess liquid water to the coolant flow channels by a pressure difference. You and Liu [8] considered liquid water concentration in a straight channel on the cathode side and concluded that a multi-phase model must be employed to obtain a more realistic simulation result.

By far, most numerical simulation models have focused on a single fuel cell or simplified stack with straight channels. Fuel cell stacks with inlet and outlet manifolds are rarely discussed. In addition, flow behaviour of unsteady, two-phase flow in a fuel cell stack with inlet and outlet manifolds is very different from that of a single, straight gas flow channel in steady state. Also, in the authors' knowledge, there is no literature available to address the liquid water behaviour in micro-parallel serpentine fuel cell channels except for the present authors' previous research [9] that only dealt with part of serpentine channels—the single U-shaped channel.

To meet these challenges, in this paper, a fuel cell stack cathode consisting of three serpentine unit cells with inlet and outlet manifolds is proposed to investigate the details of fluid flows and predict the distribution of liquid water among different cells. The pressure drop along different parts of the stack cathode is also presented graphically as it is significantly affected by the liquid water transport. In this work, the details of phase change and electro-chemical reaction were not considered. Based on the authors' understanding, the effect of the electro-chemical reaction inside the PEM fuel cell on the liquid water behaviour is mainly to continuously supply water. Therefore, in the present work, to simplify the complex process of real PEM fuel cell operating conditions, by considering different initial liquid water distributions, various operating conditions for a fuel cell stack could be simulated without involving details of electro-chemical reactions.

In the following, the computation domain, solution procedure and mesh independency are introduced. Then the results from the cases with different initial water distributions corresponding to different PEM fuel cell operating conditions are presented. Finally, conclusions are drawn and some valuable design and optimization related suggestions are given.

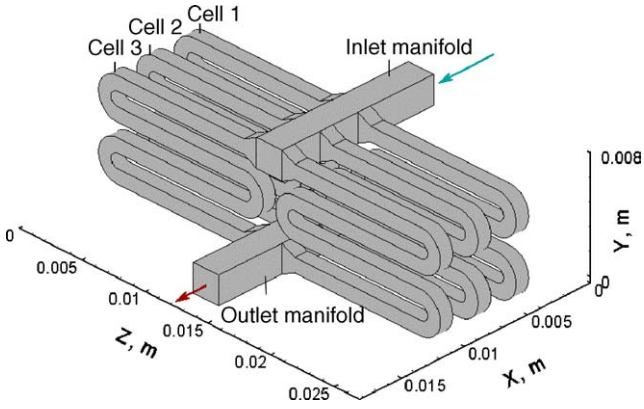

Fig. 1. Computation domain.

2. Numerical model setup

2.1. Computation domain and boundary conditions

Fig. 1 illustrates a schematic of the computation domain showing the cathode side of the three-cell parallel serpentine PEM fuel cell stack considered with the inlet and outlet flow manifolds at the top and bottom, respectively. Both manifolds were 12 mm long and had a cross-section of 2 mm × 2 mm with three serpentine unit cells connected between them. Each unit cell had two symmetric serpentine gas flow channels with a cross-section of 1 mm × 1 mm and the straight section of the gas flow channels was 10 mm long. The isothermal air–water transport process inside the computation domain was modeled as a 3D two-phase viscous laminar flow. A no-slip boundary condition was applied to the surrounding walls. A velocity inlet boundary condition (uniform air velocity distribution of 10 m/s with a direction normal to the inlet boundary) was applied at the air inlet of the inlet flow manifold. At the outlet, the boundary condition was assigned as outlet flow (the gradients of all flow properties are zero). Gravity was taken as being along the negative *y*-direction. To simulate liquid water behaviour under various PEM fuel cell operating conditions, the initial water distribution inside the computation domain was carefully setup and the details are given in Section 3.

2.2. Computational methodology

The numerical simulations of the 3D, unsteady, laminar, multi-phase flow in the computation domain was performed using FLUENT [10]. An inspection of the numerical setup revealed that the Reynolds number in the model was less than 1400, thereby supporting laminar flow assumption. No energy equations were considered therefore the conservation of mass and momentum were the governing equations for the model. To track the air–water two-phase flow interface inside the computation domain, the volume-of-fluid (VOF) [10] method implemented in FLUENT was used. The VOF model is designed for two or more immiscible flu-

ids, where the position of the interface between fluids is of interest.

Then the conservation laws of mass and momentum governing unsteady, laminar flow could be written as [10]:

Continuity equation:

$$\frac{\partial \rho}{\partial t} + \nabla(\rho \vec{v}) = 0 \quad (1)$$

Momentum equation:

$$\frac{\partial(\rho \vec{v})}{\partial t} + \nabla(\rho \vec{v}\vec{v}) = -\nabla p + \nabla(\bar{\bar{\tau}}) + \rho g \quad (2)$$

where p is the static pressure, and $\bar{\bar{\tau}}$ is the stress tensor, which is given by:

$$\bar{\bar{\tau}} = \mu[(\nabla \vec{v} + \nabla \vec{v}^{\mathrm{T}}) - \tfrac{2}{3}\nabla \vec{v} I] \quad (3)$$

where I is the unit tensor.

Volume fraction of liquid water (α_2) could be solved by:

$$\frac{\partial \alpha_2}{\partial t} + \vec{v}\nabla\alpha_2 = 0 \quad (4)$$

Then the volume fraction of air (α_1) could be calculated by using the relation:

$$\alpha_1 + \alpha_2 = 1 \quad (5)$$

All the other properties (e.g., viscosity) could be computed in a volume-fraction weighted-average manner as:

$$\mu = \alpha_2\mu_2 + (1 - \alpha_2)\mu_1 \quad (6)$$

2.3. Validation of grid independency

There were 198, 144 cells meshed in the computation domain. Fig. 2 shows the mesh on the y–z plane. Each cell in the straight channel sections had the same size with dimensions 0.2 mm × 0.2 mm × 0.2 mm (along x, y, and z directions, respectively). Trapeziform cells were employed to generate the corners of the serpentine gas flow channels. Grid independency was tested by increasing and decreasing the number of grid cells by 20 and 50% for case 1 (as shown in Table 1). The flow phenomena of liquid water and the velocity field were almost the same. The difference in results for the different mesh systems is so small that it is negligible.

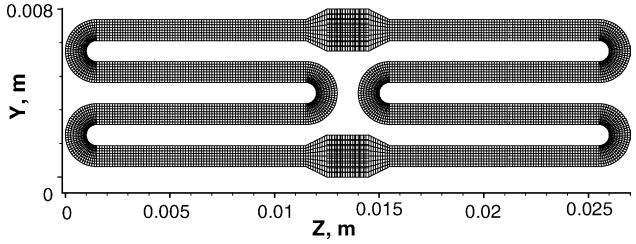

Fig. 2. Mesh on y–z plane.

3. Results and discussions

In order to investigate two-phase flow behaviour inside the parallel serpentine three-cell stack with manifolds, four different cases corresponding to four different PEM fuel cell stack operating conditions were simulated, as listed in Table 1 and shown in Fig. 3. Detailed results and discussions are given below.

3.1. Case 1: five spherical droplets freely suspended in the inlet manifold

The first case was simulated to consider small amount of water transport and distribution. As shown in Fig. 3a, five freely suspended water droplets with radius of 0.2 mm were placed along the centerline of the inlet manifold. The water distribution in different cells and manifolds, water transport in the serpentine unit cells, pressure drop along different volumes, and deformation of small water droplets were studied.

3.1.1. Water droplets deformation

Fig. 4 shows water droplet behaviour versus time as the droplets travelled through the inlet manifold on the vertical center-plane with $z = 0.0135$ m. At $t = 0$, five freely suspended droplets, with their original spherical shape, were placed in the inlet manifold. Subsequently, droplet deformation along

Table 1
Four simulated cases for different PEM fuel cell operating conditions

Case no.	Inlet velocity (m/s)	Initial water (mm^3)	Initial water distribution	Corresponding PEM fuel cell stack operating condition
1	10	0.628	Five spherical droplets ($r = 0.2$ mm) freely suspended along the central line of the inlet manifold	Fundamental study of water droplet deformation inside gas flow channels; liquid water injection at the cathode inlet
2	10	6.875	Water films with a thickness of 0.2 mm attached to surrounding walls near the manifold inlet	Excessive liquid water condensed on manifold inlet surface
3	10	37.06	Water films with a thickness of 0.2 mm placed on the windward (left) side surface of each gas flow channel in the unit cells	Most of the liquid water generated on the windward side surface (MEA located here) of each unit cell gas flow channel
4	10	37.06	Water films with a thickness of 0.2 mm placed on the leeward (right) side surface of each gas flow channel in the unit cells	Most of the liquid water generated on the leeward side surface (MEA located here) of each unit cell gas flow channel

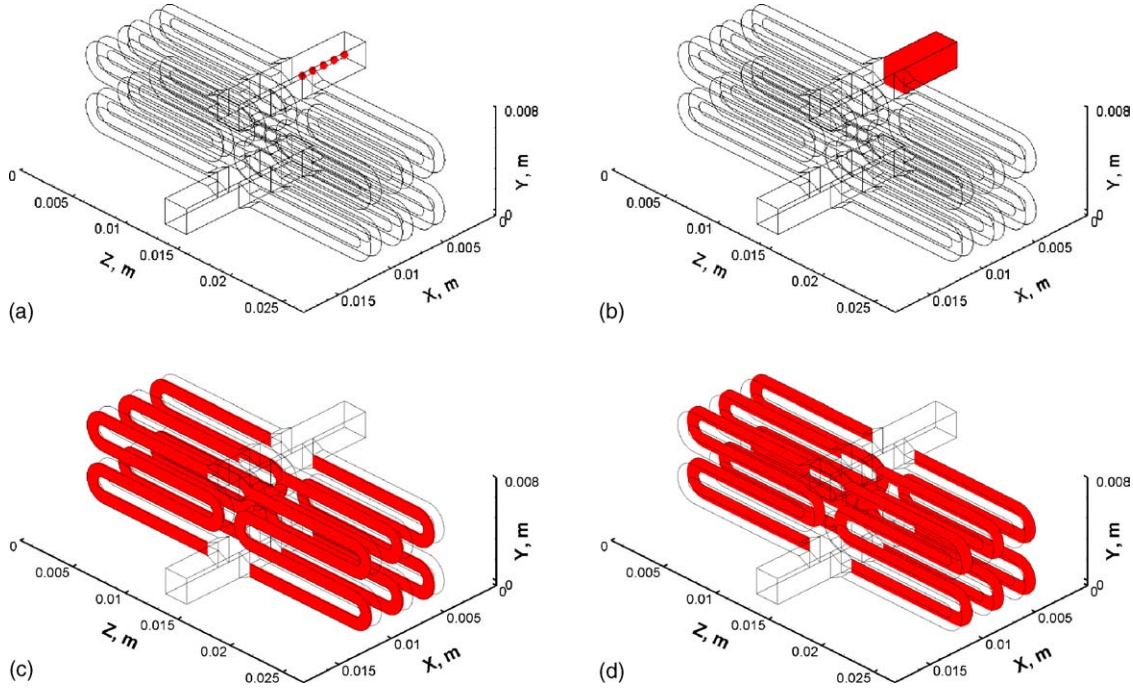

Fig. 3. Initial water distribution for the four cases (a: case 1; b: case 2; c: case 3; d: case 4).

the x-direction, attributable to effects of dragging force from the airflow, could be noticed. Since the size of the water droplets was very small, the effect of gravity was not significant. The droplet on the far right section (near the inlet) had the largest deformation along the x-direction. However, the droplet on the far left section had its original spherical shape and was only slightly elongated along the x-direction. Because airflow originated at the inlet, the interaction between airflow and the water droplets was significant for the droplet on the far right section (near the inlet). Furthermore, the droplet on the far right section blocked some of the airflow resulting in reduced airflow effects on the other droplets. In other words, shear stress on the droplets would keep decreasing along the main flow direction (to the left in Fig. 4) and correspondingly, the droplets on the left side would maintain their original shapes rather than deforming. Therefore, it could be concluded that the droplets closest to the air inlet suffered the largest air dragging forces than the droplets far away from the air inlet.

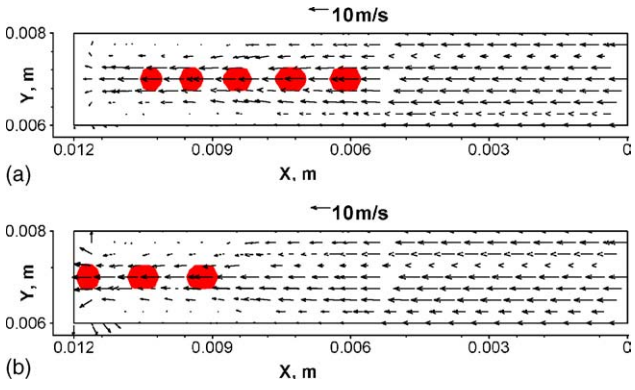

Fig. 4. Water distribution and velocity field on the vertical center-plane ($z = 0.0135$ m) in the inlet manifold for case 1 (a: $t = 0.006$ s; $t = 0.009$ s).

3.1.2. Water amount distribution and its effects on velocity fields

When the water droplets approached the end wall (at $x = 0.012$ m) of the inlet manifold, the velocity field at the near-wall surfaces would change with liquid water displacement. Fig. 5 shows how the velocity field was affected by liquid water movement on the plane close to $x = 0.012$ m. The upper section of this figure shows the cross-section of the inlet manifold, it also shows that airflow was reflected at the near-wall surfaces. With water approaching the surface, the velocity increased due to the squeeze effect between the wall and the water droplets and hence forced all the liquid water to expand to both sides along the z-direction (Fig. 5b). Simultaneously, water would be divided into two parts to the both sides of the gas flow channels. The lower section in this figure shows the cross-section of the outlet manifold. The two outgoing air streams flowing out of the gas flow channels squeezed each other. After water spread to the gas flow channels, as shown in Fig. 5c, there is still a small amount of water adhering to the wall, attributable to the effect of wall adhesion and the stagnant effect.

Water distribution in 3D view was shown in Fig. 6, it could be observed that there was almost no water travelling through the cells 1 and 2. In other words, the water was not evenly distributed among all the cells. Fig. 7 describes the relative amount of water in different cells and manifolds, cells 1 and 2 had zero variation of water amount. There was no water flowing into these two cells and the water amounts remained

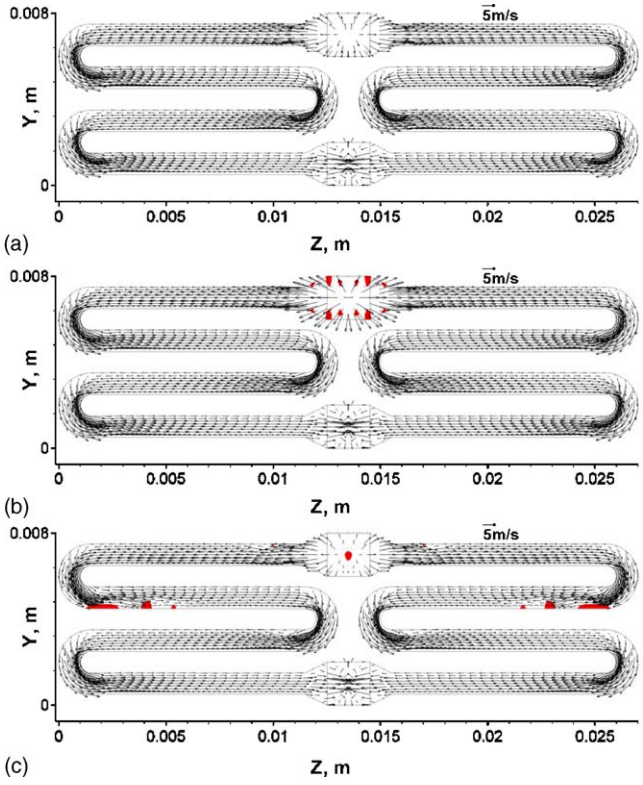

Fig. 5. Water movement on the plane close to the wall at $x = 0.012$ m for case 1, the inlet manifold is at the top and the outlet manifold is at the bottom (a: $t = 0.0003$ s; b: $t = 0.0009$ s; c: $t = 0.006$ s).

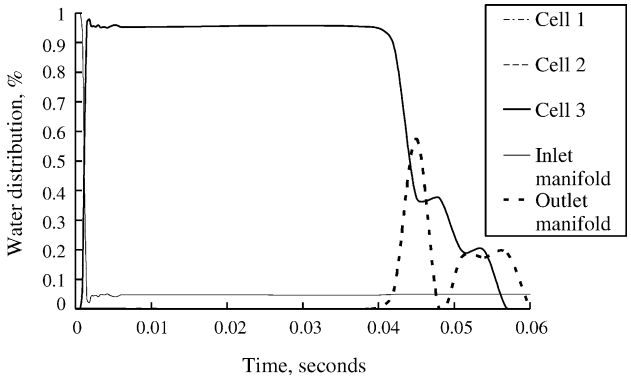

Fig. 7. Water amount variation in different cells and manifolds for case 1.

zero all the time. From Fig. 6, it was observed that all the five water droplets were flowing onto the end wall ($x = 0.012$ m) facing the air inlet. Eventually, water started spreading on that wall and moved into cell 3. Fig. 7 also shows the process from 0.0008 to 0.0015 s during which the amount of water in the inlet manifold decreased rapidly, while increased in cell 3. Subsequently, the water amount in these two volumes remained constant for a while, while water was flowing through cell 3. It could also be observed that there was about 4% of water remained in the inlet manifold. Also in cell 3, the relative water amount remained about 96% for most of the time. As mentioned earlier, this was due to the wall adhesion, and some of the water hitting that wall would stick onto it, as shown in Figs. 5c and 6. Also Figs. 5 and 6 show that even the outgoing air streams were trying to squeeze each other in the outlet manifold, water still moved toward the

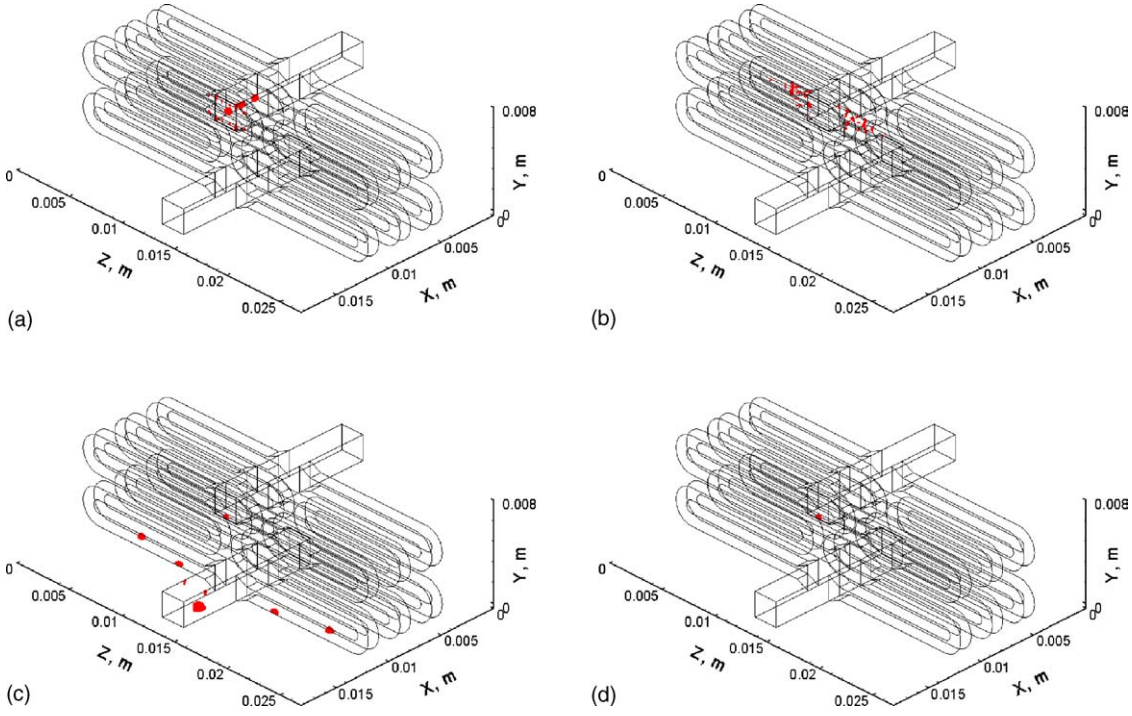

Fig. 6. Water movement in 3D view for case 1 (a: $t = 0.0009$ s; b: $t = 0.0015$ s; c: $t = 0.045$ s; d: $t = 0.06$ s).

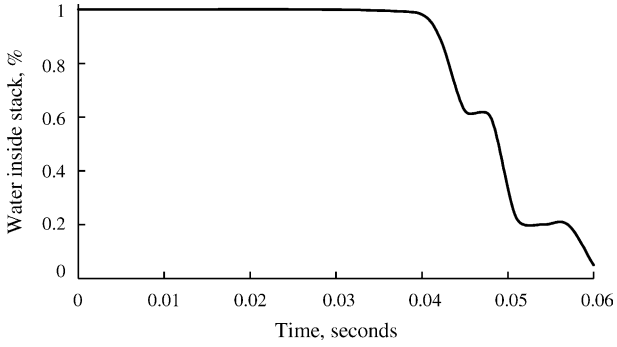

Fig. 8. Water amount inside stack vs. time for case 1.

outlet, which is good for water drainage. The overall water amount inside the cathode (stack) versus time is shown in Fig. 8, at $t = 0.04$ s, water started moving out from the stack indicated by the decrease of the curve. This curve decreased three times, this means water was collected and separated into three parts to flow out of the channel, this could also be observed from Fig. 6c. The "collecting-and-separating-effects" from the serpentine shape will be discussed further in the next three cases. Generally, it was found that it is difficult to attain an even water distribution for these kinds of parallel gas flow channels. And once most of the water has moved into one cell, the performance of the fuel cell would decrease due to either unstable operation or water flooding.

3.1.3. Pressure drop change due to water movement inside the inlet manifold

Fig. 9 shows the pressure drop along different volumes for case 1. It could be observed that the pressure drop along cell 3 was always greater than that along cells 1 and 2. Recalling the general calculation of pressure drop along a horizontal pipe without considering gravity force (gravity effect is minor factor for the present study due to the size of droplets and small amount of liquid water) [11], we have equation:

$$\Delta p = f \frac{l}{D} \frac{\rho V^2}{2} \tag{7}$$

with f is the friction factor, l the length, D the hydraulic diameter and V the velocity. For all the three single cells, they

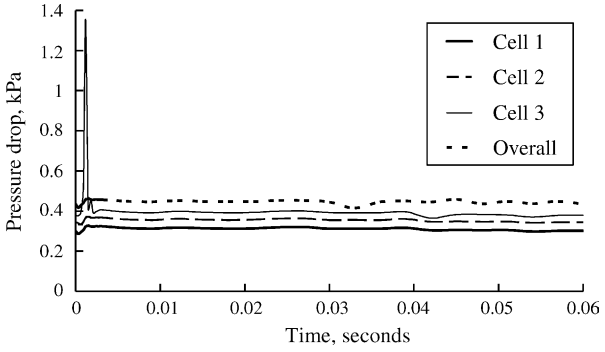

Fig. 9. Pressure drop along different volumes for case 1.

have the same geometry, thus the main factor that affect the pressure drop is the water amount. Different water amount in the single cell would change the available cross-section area of the channel for gas to pass through and thus the gas flow velocity would be different. At $t = 0$, there was no water in the three single cells, the pressure drop in cell 3 is still the highest, this means that cell 3 always had a greater flow rate of air than the other two cells, and cell 3 could be the easiest one to flow in. At about 0.001 s, while water hit the wall facing the air inlet, the pressure drop along cell 3 increased significantly. This is because air was squeezed from the end wall ($x = 0.012$ m) by water hitting on it. As all that water moved into the cell, the pressure drop decreased. Cell 3 always has a greater pressure drop than that of the other two cells, it could be considered as the unit cell with the highest possibility of having most of the water flowing through (as in this case). This would also be demonstrated in the next three cases.

3.2. Case 2: water films with a thickness of 0.2 mm attached to the surrounding walls near the manifold inlet

Four water films with thickness of 0.2 mm were attached to the surrounding walls, as shown in Fig. 3b. All the water films were 5 mm long. Water was expected to move into all the three unit cells, the variations of water amount and pressure drop in each volume could perform more significantly.

3.2.1. Water "flowing backward"

Fig. 10 shows the water transport and velocity field on the vertical center plane with $z = 0.0135$ m of the inlet manifold. The gravity force acts in the negative y-direction. At $t = 0.0003$ s, the water films were already flowing away from the air inlet. Part of water close to the air inlet was slightly lifted up by the air stream. The amount of water was small for such an air stream to have gravity effects significantly shown in the figure. At a later time, water hit the end wall that faces the air inlet, and air was squeezed from the end wall at $x = 0.012$ m. There were two vortices formed at the top and bottom of the inlet manifold, as water approached the wall, as shown in Fig. 10a and b, the vortices were squeezed and the velocity vectors directed toward the air inlet became much stronger. Water started moving back to the air inlet as shown in Fig. 10c and d. At $t = 0.009$ s, some water already moved half way in the inlet manifold (Fig. 10d). Because air was continuously flowing from the air inlet, therefore, water was flowing downstream again to the end wall, as shown in Fig. 10e. During this time period, gravity effects gradually became important and could be noticed as shown in Fig. 10c through f. When this part of water moved back to the end wall at $x = 0.012$ m, it already moved down to the bottom surface of the inlet manifold and adhered to the surrounding walls as shown in Fig. 10f. The reason that some water flowed backwards after hitting the end wall of the inlet manifold is because water was reflected from this wall. While water started moving back, the air flow resistance was not significant, as shown in Fig. 10c, the velocity filed on the left

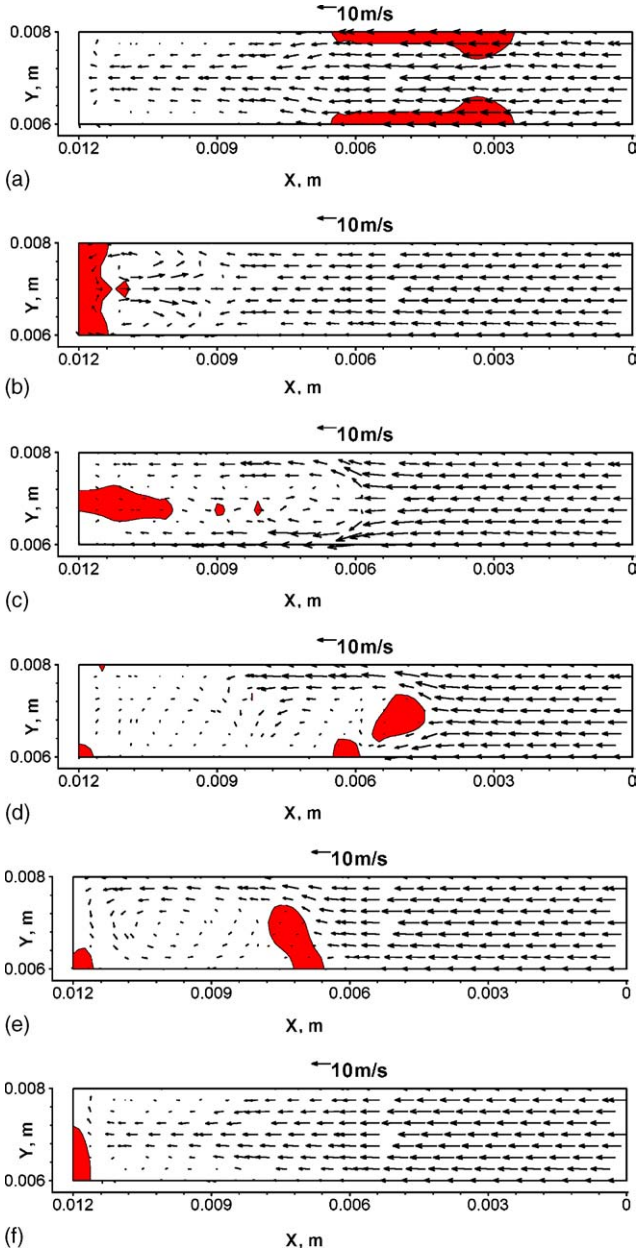

Fig. 10. Water distribution and velocity field on the vertical center-plane (z = 0.0135 m) in the inlet manifold for case 2 (a: t = 0.0003 s; b: t = 0.0012 s; c: t = 0.0024 s; d: t = 0.009 s; e: t = 0.012 s; f: t = 0.018 s).

side of the water is very small; this is because there are other channels that air could move into (cells 1 and 2). Therefore, water could flow backward to the air inlet for such a long distance.

3.2.2. Water amount variation

Fig. 11 shows water movement in 3D view, as time progressed, different from the first case; water was distributed to all the three cells. Fig. 12 shows the variation of water amount in different volumes. For most of the time, cell 3 had the largest amount of water (about 65% of total amount of initially loaded water). Cell 1 with about 15% total amount of initially loaded water was slightly more than that in cell 2 (10%). From Fig. 11d, it could be observed that some water remained on the end walls of both the inlet and outlet manifolds. With help of Fig. 12, at time t = 0.08 s, we could find that about 10% of water sticking on the end wall of the inlet manifold, and 4% sticking on the end wall of the outlet manifold. The reason that we have water sticking on the end wall of inlet manifold was discussed in case 1. The water transport in the outlet manifold will be discussed in the next section. The variation of overall water amount inside the cathode (stack) was shown in Fig. 13. The decreasing curve is similar to Fig. 8 for case 1, the reason that the curve is decreasing step by step is because water was collected and separated into several parts through the serpentine flow channels. In this case water started moving out of the stack at about 0.032 s, this is earlier than that in case 1. At last, water amount remained at about 14%, which represents the water in both the inlet and outlet manifolds.

3.2.3. 'Squeezing' of water in the outlet manifold

Fig. 14 shows the vertical center plane with z = 0.0135 m of the outlet manifold. Water flowed into the outlet manifold from both sides of the gas flow channels and then would amalgamate on this plane. The air streams from both sides of gas flow channels would also squeeze each other on this plane. As shown in this figure, as time progressed, water was flowing onto this plane and then was squeezed to move along both the positive- and negative x-directions. After that, this part of water was tearing up, as shown in Fig. 14c. At a later time, as shown in Fig. 14d and e, some water from cell 1 moved onto this plane, after being squeezed to both sides along the x-direction, some water moved onto the end wall (x = 0.005 m) of the outlet manifold and adhered to it. Therefore, due to the effect of wall adhesion and surface tension, the water sticking on this wall would be hard to move to anywhere else, thus explaining why some water remained in the outlet manifold.

3.2.4. Comparison of both pressure drop and flow behaviour of cases 1 and 2

As shown in Fig. 15, the pressure drop changed more dramatically in case 2, just note that the smaller graph in this figure represents the first 0.003 s period that could not be clearly shown in the main graph. Within the first 0.003 s, the pressure drop increase occurred in all the three unit cells while water passed the inlet of the three cells. Pressure drop increase first occurred at cell 1 and then cell 2, with almost the same magnitude of 6 kPa. While such a large amount of water flowing through, air could be squeezed and the pressure at the inlet would increase significantly, this was also mentioned in case 1. The pressure drop increase in cell 3 occurred later, but with the largest magnitude of 25 kPa. This is because there is an end wall (x = 0.012 m) at the inlet of this cell. As the water hit this wall, the squeezing effect would become more significant thus increasing the pressure. By looking at the whole time period, it could also be observed that the pressure drop in cell 3 was always greater than that in cells 1 and 2. This is

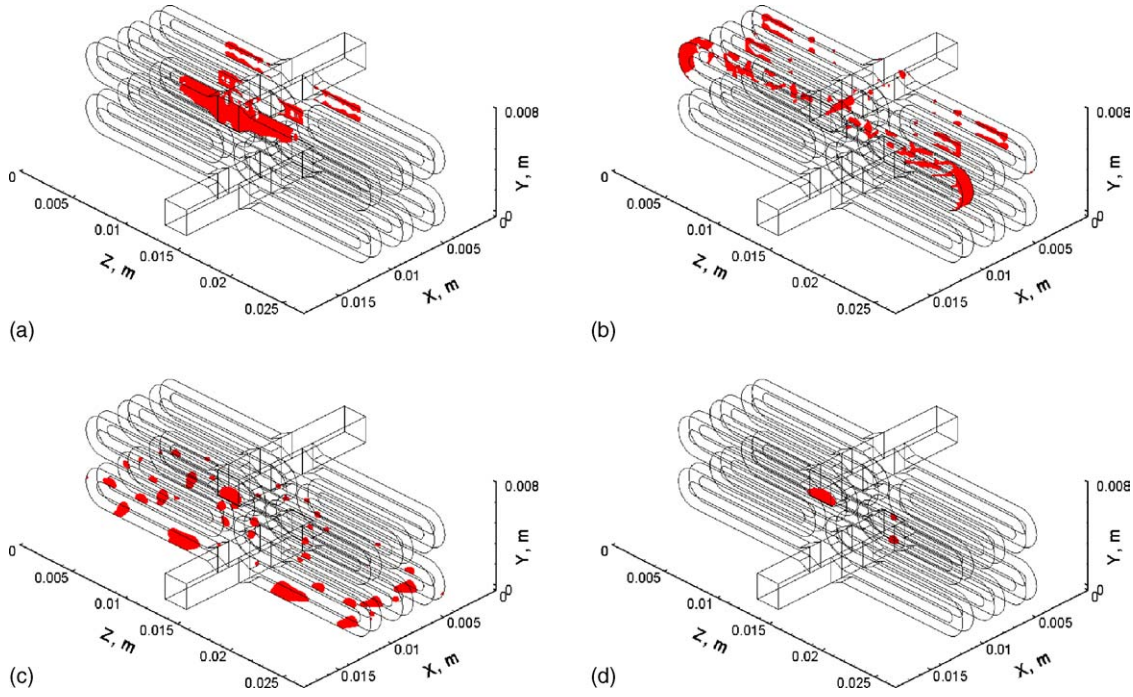

Fig. 11. Water movement in 3D view for case 2 (a: $t = 0.0015$ s; b: $t = 0.003$ s; c: $t = 0.03$ s; d: $t = 0.082$ s).

similar to the result obtained in case 1. The overall pressure drop decreased from the beginning because the water was initially flowing away from the air inlet.

By contrast, both cases 1 and 2 showed that cell 3 always had a larger pressure drop than cells 1 and 2 (Figs. 9 and 15) and most of water moved into this cell (Figs. 7 and 12). Therefore, it could be concluded that cell 3 is the most possible cell to have the largest amount of water in this kind of stack, regardless of where water was from in the inlet manifold. It was noticed that the water amount in the outlet manifold changed dramatically (Figs. 7 and 12). This is because while water flowed into the outlet manifold, there would be some water flowing out of the manifold. However, in case 2, it could be noticed that finally this curve remained at about 4%, as shown in Fig. 12, indicating that there was some water remained in the outlet manifold. As discussed before, this was because some water passed through cell 1 in case 2.

By comparing the flow behaviours in the first two cases, as mentioned before, it is difficult to have evenly distributed water among the three unit cells. In this kind of stack, the last cell (cell 3) that is furthest away from the air inlet and connecting the end wall of the inlet manifold would always have the greatest pressure drop and the largest amount of water distribution from the inlet manifold. By investigating the velocity fields in the outlet manifold in both cases 1 and 2, it was found that the outgoing air streams from the three cells were blocking and squeezing the water in the outlet manifold. So water from cell 3 would always be the easiest path for water to flow out from the stack, because this part of water would encounter the weakest resistance. Therefore, it could be concluded that, if the unit cell further away from the gas flow outlet had greater water distribution, then the water flowed out from this unit cell would be blocked by the air streams from the other unit cells.

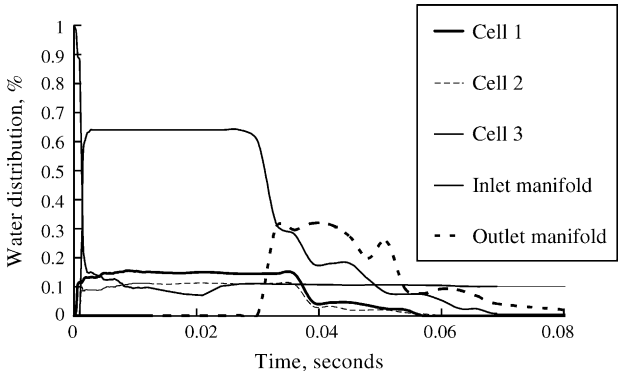

Fig. 12. Water amount variation in different cells and manifolds for case 2.

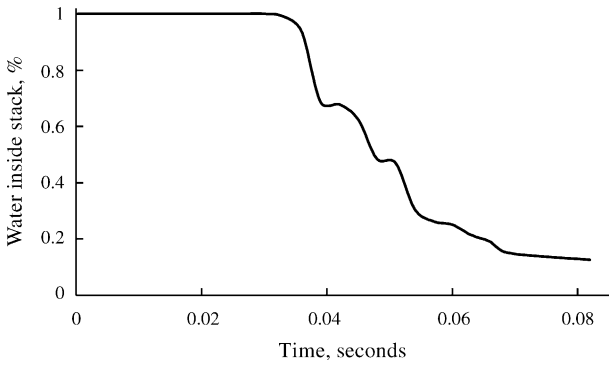

Fig. 13. Water amount inside stack vs. time for case 2.

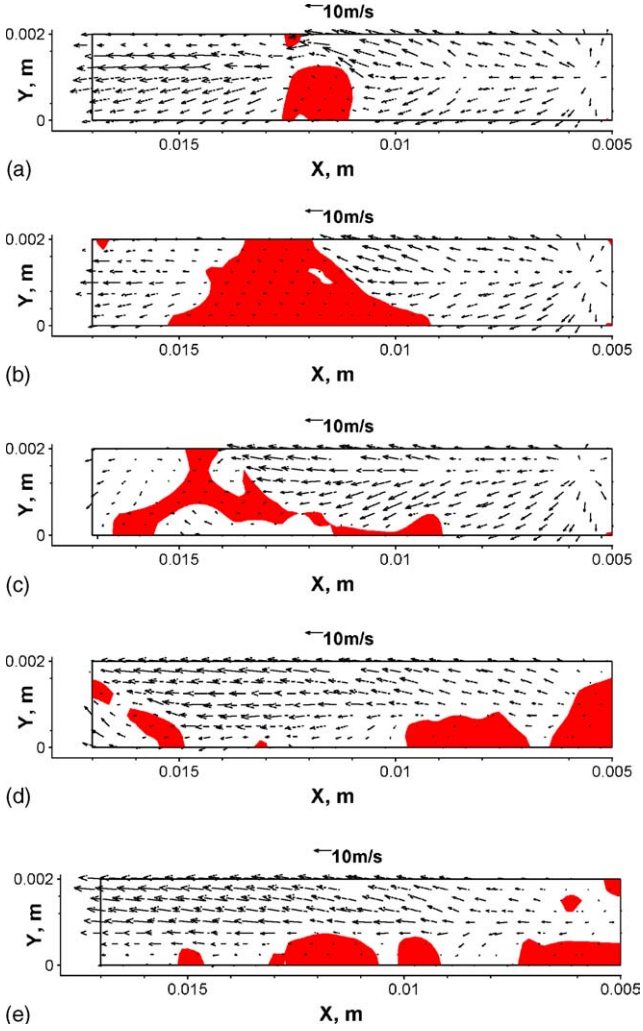

Fig. 14. Water distribution and velocity field on the vertical center-plane (z = 0.0135 m) in the outlet manifold for case 2 (a: t = 0.033 s; b: t = 0.0345 s; c: t = 0.036 s; d: t = 0.0375 s; e: t = 0.039 s).

On the contrary, better water draining conditions could be achieved when the unit cell(s) closest to the gas flow outlet has (have) the largest water distribution, as in cases 1 and 2.

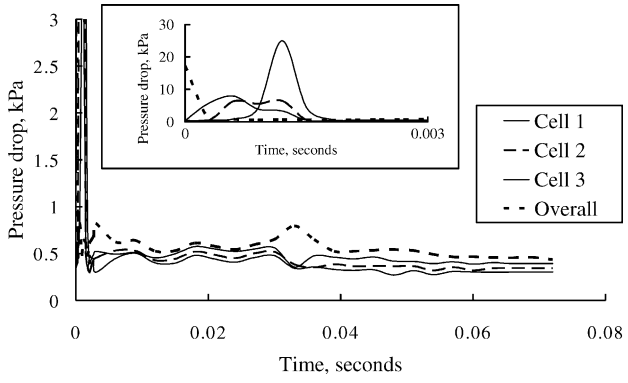

Fig. 15. Pressure drop along different volumes for case 2.

3.3. Case 3: water films with a thickness of 0.2 mm placed on the windward (left) side surface of each gas flow channel in the unit cells

In case 3, the windward (left) side surface of each gas flow channel was covered with a water film with a thickness of 0.2 mm. These surfaces were assumed to be the electrode surfaces of the gas flow channels on the cathode side, on which water films could be formed by electro-chemical reactions and water vapour condensation during PEM fuel cell operations. Here the electro-chemical reaction was not considered while the water film was used to simulate water production as stated in Section 1 of this paper. The initial water distribution is shown in Fig. 3c for case 3.

3.3.1. 'Collecting-and-separating-effect" in serpentine gas flow channel

Fig. 16 shows how generally water was transported through the cell stack. At t = 0.0006 s, water in the gas flow channels was separated into different parts by the U-shaped corners (U-turns). This is because the water approaching the U-turns would slow down and hit on the U-turn outside surface due to the inertia effect, but the water leaving the U-turn would resume its normal speed in the horizontal channel. Therefore, the water after the U-turns would move faster than the water coming to the U-turns. Thus that water was "separated" by the U-turn was explained. On the other hand, because the water coming to the U-turns moved slowly, this part of water would wait for the water leaving from its upstream U-turn. Therefore, at the U-turns of the serpentine gas flow channels, water was also "collected". Generally speaking, at the U-turns of the serpentine gas flow channels, water was collected and then separated into different parts. When the water films were separated into small droplets, it would be much easier to remove them. Therefore the serpentine design actually can facilitate the water removal by using its "collecting-and-separating-effect". This is just like the military strategy "divide and conquer". In Fig. 17, at t = 0.0006 s, it could be noticed that the velocity fields and water distribution were almost the same on the near-wall surfaces of the three unit cells (water in cell 3 moved a little bit faster). Therefore, it could be expected that water in the three unit cells would have similar transportation characteristics. This could be appreciated with the help of Fig. 18, which shows the water amount variation along different unit cells and manifolds. In particular this case (case 3), since a relatively large amount of water was considered as evenly distributed in the gas flow channels, the water in the inlet manifold would always be maintained at zero. As shown in Fig. 18, water in the three unit cells had the same amount of initial water distribution, and moved into the outlet manifold within almost the same time period (cell 3 was slightly faster), it could also be noticed that the curve representing the water amount in the three unit cells decreased step by step, which is similar as in Figs. 8, 13 and 19. The reason is as we mentioned, water was separated into several parts by the U-turns. Fig. 19

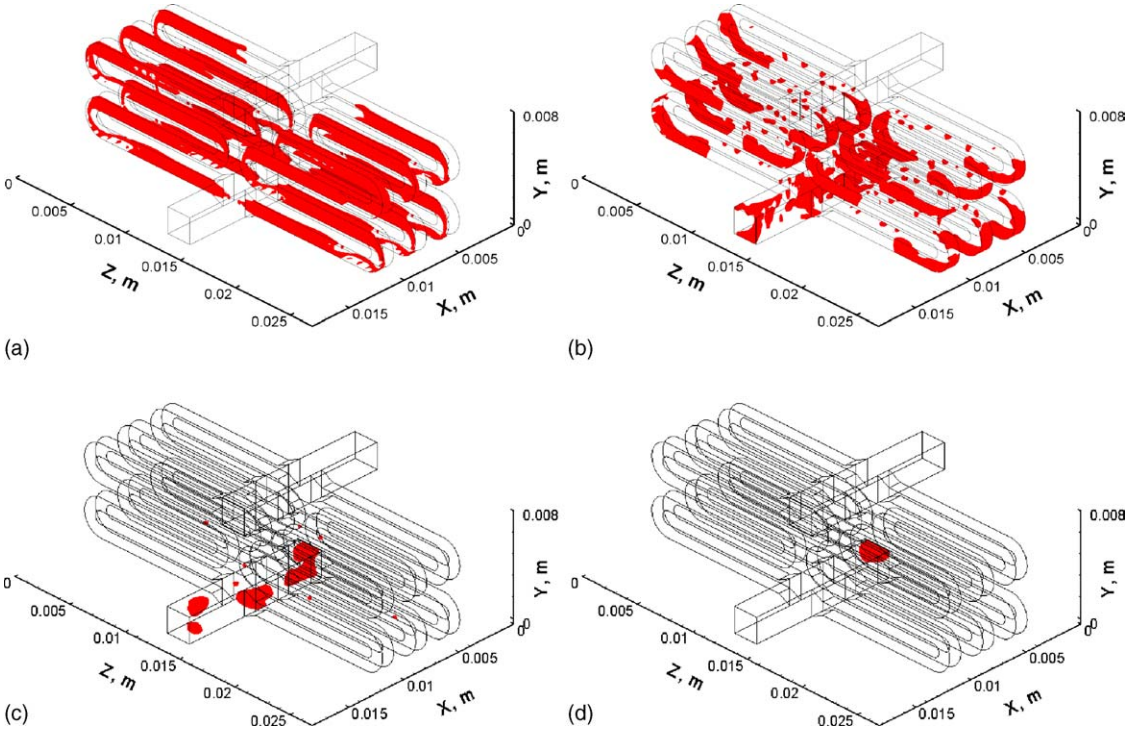

Fig. 16. Water movement in 3D view for case 3 (a: $t = 0.0006$ s; b: $t = 0.003$ s; c: $t = 0.039$ s; d: $t = 0.075$ s).

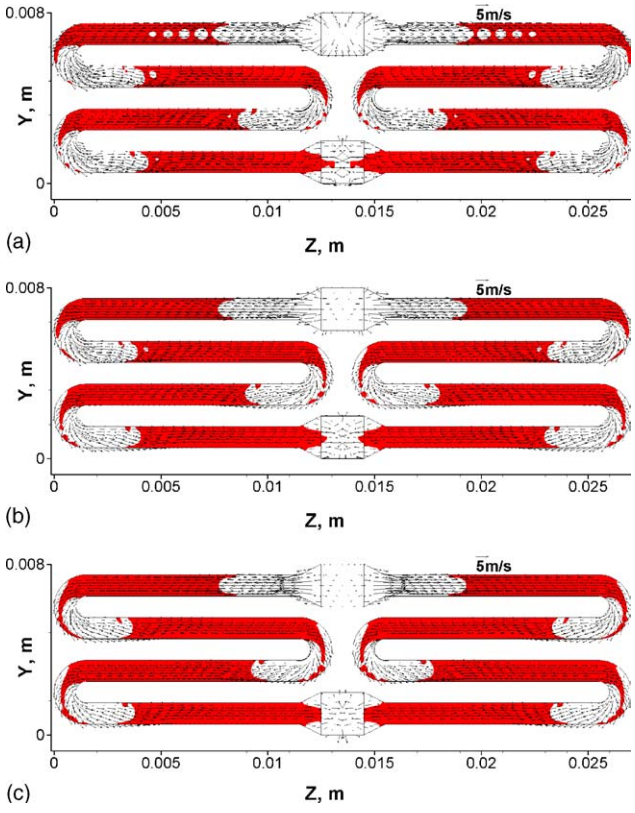

Fig. 17. Water on the near-wall surfaces at $t = 0.0006$ s for case 3 (a: $x = 0.012$ m; b: $x = 0.009$ m; c: $x = 0.006$ m).

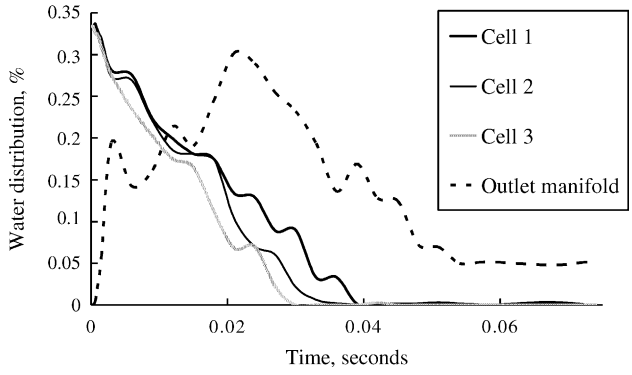

Fig. 18. Water amount variation in different cells and manifolds for case 3.

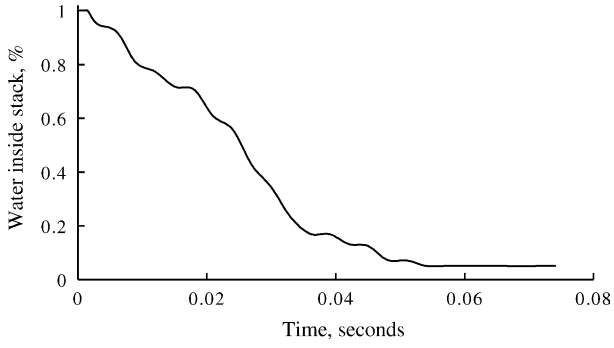

Fig. 19. Water amount inside stack vs. time for case 3.

shows the overall water amount inside cathode (stack), the curve decreased step by step as in Figs. 8 and 13. Fig. 19 also showed that water started moving out of the stack at about 0.015 s.

At $t = 0.04$ s, as shown in Fig. 18, water in the three unit cells was already flown away, and the three curves maintained at almost zero. Even though the difference was not significant, the results showed that cell 3 had a better water draining ability than cells 1 and 2. At a later time, as shown in Fig. 16b, water was not just maintained on the windward wall of the unit cells, most of the water moved onto the bottom surfaces and even the leeward surfaces. It is not easy to ascertain to which surface water would adhere in such a long time period; this depends on different factors such as shape of the flow channels, airflow velocity, among others. The outlet manifold still had excessive water left which was about 5%, as shown in Figs. 16d and 18. This is because some of the water from cell 1 was squeezed onto the end wall of the outlet manifold. The same phenomenon was shown in case 2 (Figs. 11d and 12).

3.3.2. Change of pressure drop when the outlet manifold blocked with water

The pressure drop in different volumes for this case is shown in Fig. 20. Different from case 2, the pressure drop decreased in all the three unit cells within the first 0.003 s. This is because as the water flowed into the outlet manifold, the increasing amount of water in the outlet manifold would block the outlet of each unit cell, the pressure in the outlet manifold and the outlets of the unit cells could become very high. Therefore, the pressure drop along the unit cells decreased. The pressure drop decreased first in cell 3, then cells 2 and 1. In cell 3, the pressure drop only decreased by about 0.4 kPa, and only for a little while, this is because cell 3 is easier for the water coming out from it to flow into the outlet manifold (as was concluded in case 2). But later, the pressure drop decreased more in cells 1 and 2, by about 1 kPa, this is because water flowed out from these two cells could be blocked by the outgoing air streams from cell 3, and the end wall ($x = 0.005$ m) of the outlet manifold was connecting to cell 1, then due to the effect of wall adhesion, water coming out from cell 1 could be more difficult to move out of the stack. Therefore, more water could stay in the outlet manifold at the outlets of cells 1 and 2, and the pressure here could become very high. This explained why the pressure drop decreased severely in cells 1 and 2. At about 0.0022 s, in Fig. 20, while the pressure drop in cells 1 and 2 decreased, it could be observed that the pressure drop in cell 3 increased simultaneously. Recalling from Eq. (7), we know that the flow rate or velocity is the main factor that affects the pressure drop. Therefore, while air had difficulty to flow through some gas flow channels (cells 1 and 2), more air would flow through the other cells (cell 3), thus decreasing the pressure drop along cells 1 and 2 and increasing the pressure drop along cell 3. The overall pressure drop also increased during this time period, because with the unit cells blocked, the pressure in the inlet manifold would be increased, thus increasing the overall pressure drop. At a later time, by looking at the overall time period, it could be observed that the pressure drop changed dramatically, but the pressure drop in the three unit cells never decreased or increased together. This is because when some unit cells have less air flowed in (the pressure drop would decrease), other unit cells would always have a much higher flow rate (the pressure drop would increase) to maintain the mass conservation. This could be observed in Fig. 20. Generally, by looking at the overall pressure drop in Fig. 20, it could be observed that cell 3 still had a greater pressure drop than the others, and after 0.05 s, as all the water flowed out of the cells, the pressure drop in the three unit cells remained constant and cell 3 still had its greatest magnitude.

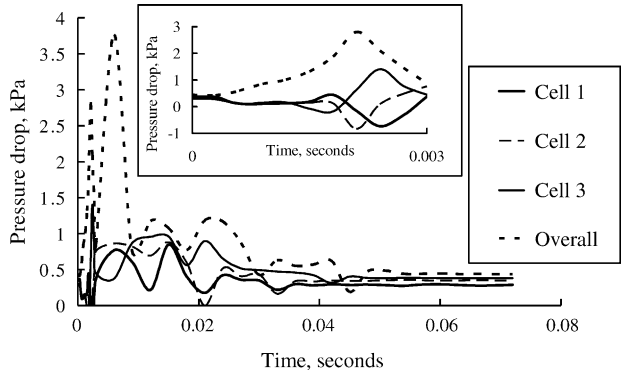

Fig. 20. Pressure drop along different volumes for case 3.

3.4. Case 4: water films with a thickness of 0.2 mm placed on the leeward (right) side surface of each gas flow channel in the unit cells

Case 4 was simulated to compare with case 3. In this case, the MEA side was assumed to be windward (on the left hand side), as shown in Fig. 3d. Therefore, the water films formed due to electro-chemical reactions would be assumed on this side and the initial water distribution is shown in Fig. 3d.

3.4.1. Comparison of water flow behaviours in cases 3 and 4

Similar to case 3, water was initially broken up at the U-turn, as shown in Figs. 21 and 22. The "collecting-and-separating-effect" could also be noticed. As time passes, water in the gas flow channels moved to other surfaces, this is also similar to case 3. Also as shown in Fig. 22, the water distribution and velocity fields were almost the same on the leeward surfaces for the three unit cells. After water moved away, it could be noticed that there was some water remained on the end wall of the outlet manifold; this was shown in cases 2 and 3 too. Therefore, the authors concluded that, once there is water flowing through the gas flow channels closest to the end of wall (the wall facing and furthest away from the air flow outlet), it is unavoidable to have some water adhering to this wall.

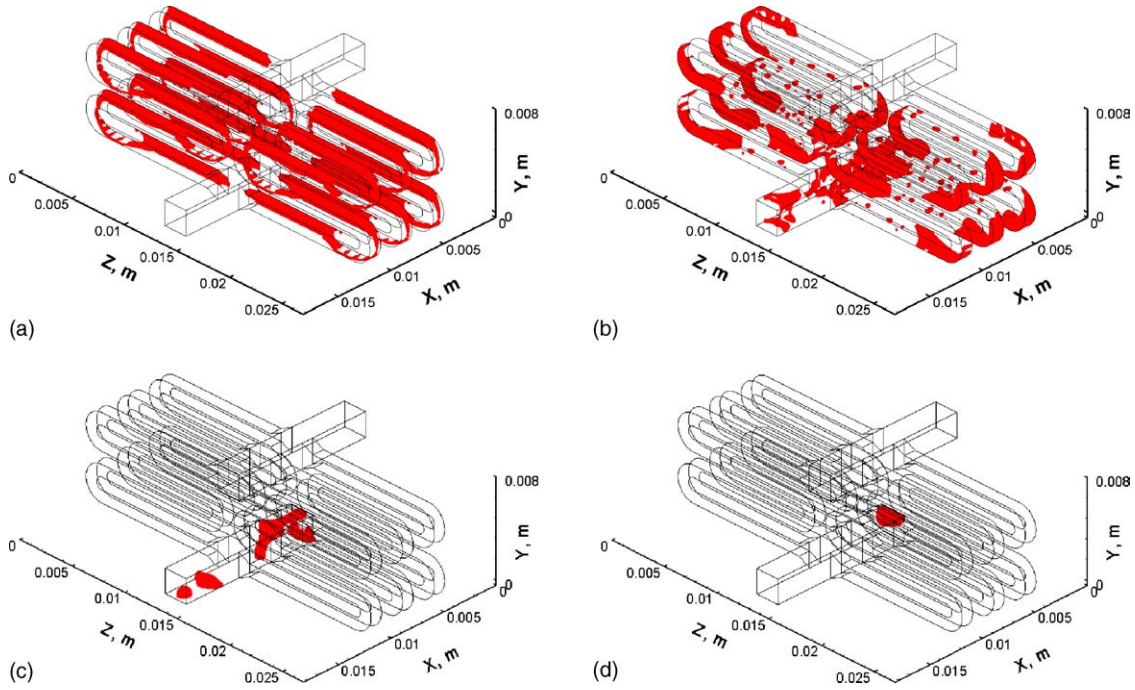

Fig. 21. Water movement in 3D view for case 4 (a: $t = 0.0006$ s; b: $t = 0.003$ s; c: $t = 0.048$ s; d: $t = 0.075$ s).

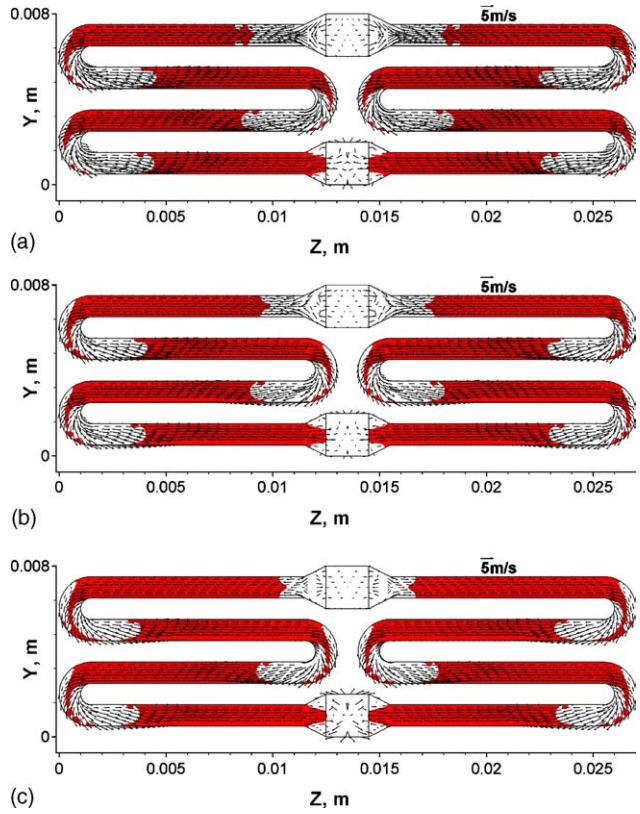

Fig. 22. Water on the near-wall surfaces at $t = 0.0006$ s for case 4 (a: $x = 0.011$ m; b: $x = 0.008$ m; c: $x = 0.005$ m).

Fig. 23 shows the water distribution along different volumes; this figure is very similar to Fig. 18. But in this case, it took a time period of 0.06 s to have all the water flow out of the gas flow channels; longer than that in case 3 which was about 0.05 s. Also if we look at the overall water amount inside cathode (stack) for case 4, as shown in Fig. 24, no significantly difference could be found by comparing to Fig. 19, both curves decreased step by step, the water flow behaviours were very similar between cases 3 and 4, the only difference is that case 3 had faster water drainage. The difference between cases 3 and 4 is the initial water film arrangement; in case 3 the water films were placed on the surfaces closer to the air outlet while in case 4 they were placed further. Better water draining was achieved by placing the water films closer to the air outlet (as in case 3), thus it could be concluded that arranging the MEA side of the unit cells closer

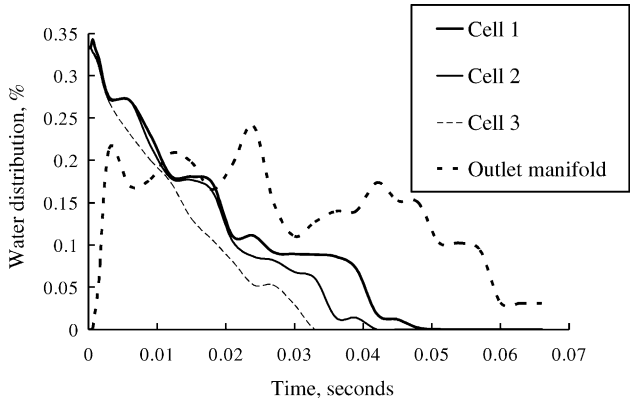

Fig. 23. Water amount variation in different cells and manifolds for case 4.

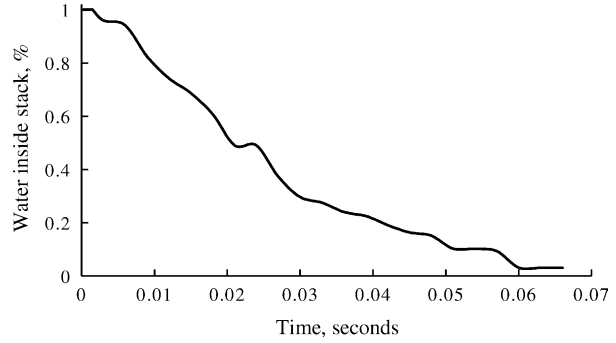

Fig. 24. Water amount inside stack vs. time for case 4.

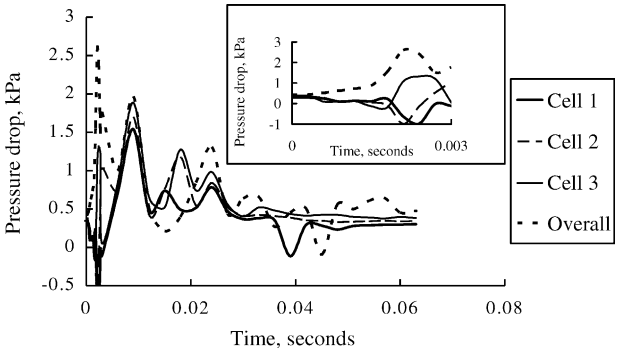

Fig. 25. Pressure drop along different volumes for case 4.

to the gas flow outlet could obtain a better water draining process.

3.4.2. Comparison of pressure drop in cases 3 and 4

As shown in Fig. 25, the pressure drop in different volumes is also similar to case 3, as shown in Fig. 20. In both figures, the pressure drop along the three unit cells never decreased or increased at the same instant, as we mentioned earlier, this is because once some cells had lower flow rate (pressure drop would decrease), other cells would have higher flow rate (pressure drop would increase). But cases 3 and 4 approved that the pressure drop along different unit cells in this kind of cell stack is very sensitive, especially with different water distribution in each cell. Once one unit cell had a lower flow rate, the pressure drop along this cell would decrease, on the other hand, as the pressure drop decreased, the other cells' pressure drop would increase due to a higher flow rate, this is the problem that is hard to be avoided in this kind of parallel gas flow channels.

4. Conclusions

The liquid water behaviours in parallel serpentine channels with manifolds on cathode side of a PEM fuel cell were studied by employing a 3D, unsteady, two-phase model in FLUENT with different initial water distributions. By investigating the flow behaviours of liquid water and airflow velocity fields, the following water management issues have been identified for this kind of fuel cell stack:

1. If the water is supplied from the inlet, it is almost impossible to have evenly distributed water in each gas flow channel for this type of serpentine stack design. The gas flow channel that is closer to the air outlet always has a greater pressure drop and water is most likely to flow through this channel. But unevenly distributed water is not good for achieving a stable fuel cell performance.
2. Water in the outflow manifold could be blocked by air streams from the gas flow channels, with water continuously flowing into the outflow manifold, the outflow manifold may be blocked, the pressure in the outflow manifold and the outlets of the unit cells could become very high. Therefore, the pressure drop and flow rate along these unit cells could decrease. In this kind of condition, the pressure drop and flow rate along other cells would become very high, the air flow would become unevenly distributed.

   Pressure drop along all the unit cells could never increase or decrease at the same pace, once pressure drop along some unit cells increase, others' pressure drop would decrease.
3. If water hits the wall that faces the air inlet, water could be moved towards the air inlet again. In this case, water could not be moved into the gas flow channels on time, and the inlet manifold may become blocked with continuously supplied water.
4. Water could adhere to the end wall of both the inlet and outlet manifolds and it is difficult to remove this part of water.
5. Wall adhesion effects could slow down the water draining process, thus reducing the fuel cell performance.

Some suggestions could be made to manage liquid water in an efficient way as follows:

1. Keeping a unit cell that may have the largest amount of water close to the outlet of the outflow manifold is good for water drainage, thus the performance could become more stable.
2. Keeping the MEA side of the gas flow channels close to the outlet of the outflow manifold is recommended for having faster water drainage.
3. The serpentine gas flow channel's "collecting-and-separating-effect" could facilitate water drainage.

Acknowledgements

The authors are grateful for the support of this work by the Auto21^{TM} Networks of Centre of Excellence (Grant D07-DFC), the Natural Sciences and Engineering Research Council of Canada (NSERC), and the Graduate School at the University of Windsor.

References

[1] J. Larminie, A. Dicks, Fuel Cell Systems Explained, Second ed., John Wiley and Sons, New York, 2000.
[2] J.S. Yi, J.D. Yang, C. King, AIChE J. 50 (2004) 2594.
[3] S. Dutta, S. Shimpalee, J.W. Van Zee, J. Appl. Electrochem. 30 (2000) 135.
[4] E. Hontanon, M.J. Escudero, C. Bautista, P.L. Garcia-Ybarra, L. Daza, J. Power Sources 86 (2000) 363.
[5] S.W. Cha, R. O'Hayre, Y. Saito, F.B. Prinz, J. Power Sources 134 (2004) 57.
[6] A.A. Kulikovsky, Electrochem. Commun. 3 (2001) 460.
[7] P.T. Nguyen, T. Berning, N. Djilali, J. Power Sources 130 (2005) 149–157.
[8] L. You, H. Liu, Int. J. Heat Mass Transfer 45 (2002) 2277.
[9] P. Quan, B. Zhou, A. Sobiesiak, Z. Liu, Water behavior in serpentine micro-channel for proton exchange membrane fuel cell cathode, J. Power Sources, in press.
[10] Fluent 6.1 User's Guide, Fluent Inc.
[11] B.R. Munson, D.F. Young, T.H. Okiishi, Fundamentals of Fluid Mechanics, Fourth ed., John Wiley and Sons, New York, 2002.